

Magnetic field dependence of asymmetry-induced transport: a new approach

D.L. Eggleston and J.M. Williams

Occidental College, Physics Department, Los Angeles, California 90041

(Dated: March 10, 2008)

A new technique is used to experimentally study the dependence of asymmetry-induced radial particle flux Γ on axial magnetic field B in a modified Malmberg-Penning trap. This dependence is complicated by the fact that B enters the physics in at least two places: in the asymmetry-induced first order radial drift velocity $v_r = E_\theta/B$ and in the zeroth order azimuthal drift velocity $v_\theta = E_r/B$. To separate these, it is assumed that the latter always enters the physics in the combination $\omega - l\omega_R$, where $\omega_R(r) = v_\theta/r$ is the column rotation frequency and ω and l are the asymmetry frequency and azimuthal mode number, respectively. Points where $\omega - l\omega_R = 0$ are then selected from a Γ vs r vs ω data set, thus insuring that any function of this combination is constant. When the selected flux is plotted versus the density gradient ∇n , a roughly linear dependence is observed, showing that the assumption is valid and that the diffusive contribution to the transport has been isolated. The slope of a least-squares fitted line then gives the diffusion coefficient D_0 for the selected flux. Varying the magnetic field, it is found that $D_0 \propto B^{-1.33 \pm 0.05}$. This does not match the scaling predicted by resonant particle transport theory.

I. INTRODUCTION

The Malmberg-Penning non-neutral plasma trap continues to be of interest both as a platform for basic plasma physics studies and for its applications in charged particle storage and manipulation[1]. While it is well established that electric and magnetic fields that break the cylindrical symmetry of these traps produce radial transport, a full understanding of the transport remains elusive. Indeed, our work, which focuses on the transport produced by applied electric asymmetries with frequency ω and axial and azimuthal wavenumbers n and l , has revealed serious discrepancies between experiment[2] and some of the predictions of theory[3].

Faced with these discrepancies, we have turned to developing an empirical model of the transport with an eye toward providing guidance for further theoretical development. A basic issue in this program is determining the magnetic field dependence of the transport. Although this scaling has been studied before[4, 5], there is no consensus of results. This may be due to the fact that the magnetic field B enters the transport physics in at least two ways. Firstly, in the zeroth order azimuthal $E \times B$ drift produced by the radial electric field $v_\theta = E_r/B$. This causes the particle guiding centers to drift around the trap axis with angular frequency $\omega_R = v_\theta/r$. Secondly, the magnetic field enters in the first order radial $E \times B$ drift produced by the applied asymmetry $v_r = E_\theta/B$. It is this drift which is responsible for the radial transport of particles. This dual dependence on magnetic field is seen, for example, in the expression for the flux Γ from the plateau regime of resonant particle transport theory[3]:

$$\Gamma = - \sum_{n,l,\omega} \frac{1}{\sqrt{2\pi\bar{v}^2}} \frac{L}{|n|} \left| \frac{cl\phi_{nl\omega}}{rB} \right|^2 \left[\frac{dn_0}{dr} + \frac{n_0}{T} \frac{dT}{dr} \left(x^2 - \frac{1}{2} \right) + \left(\sqrt{2}n_0 \frac{r\omega_c}{l\bar{v}} \frac{n\pi}{L} \right) x \right] e^{-x^2}. \quad (1)$$

Here $\phi_{nl\omega}$ is the Fourier amplitude of the asymmetry mode characterized by axial mode number n , azimuthal mode number l , and angular frequency ω , and n_0 , T , L , \bar{v} , and ω_c are the particle density, particle temperature parallel to B , plasma length, thermal velocity, and cyclotron frequency, respectively. The first order radial drift is the source of the $|cl\phi_{nl\omega}/rB|^2$ term while the zeroth order order B -dependence is contained in the variables $x = (\omega - l\omega_R)/(\sqrt{2}k\bar{v})$ and ω_c . When the Debye length is small compared to the plasma radius, the asymmetric potential in the plasma $\phi_{nl\omega}$ is also a strong function of x [6].

In this paper we apply a new experimental technique to remove the ω_R dependence and thus isolate any remaining magnetic field dependence. The technique is based on the hypothesis that the asymmetry frequency ω and ω_R always enter the transport physics in the combination $\omega - l\omega_R$. We then select from a Γ vs r vs ω data set those points where $\omega - l\omega_R = 0$, thus insuring that any function of this combination is constant. When the selected flux Γ_{sel} is plotted versus the density gradient ∇n_0 , a roughly linear dependence is observed, showing that this selected flux is at least partially diffusive. This linear dependence is roughly independent of the center wire bias ϕ_{cw} . Since in our experiment $\omega_R \propto \phi_{cw}$, this latter point shows that our technique has successfully removed any dependence on ω_R and its derivatives, thus confirming our hypothesis. The slope of a least-squares fitted line through the Γ_{sel} vs ∇n_0 data then gives the diffusion coefficient under the condition $\omega - l\omega_R = 0$ which we call D_0 . Varying the magnetic field, we find $D_0 \propto B^{-1.33 \pm 0.05}$. We then use these findings to constrain the form of the empirical flux equation.

II. EXPERIMENTAL DEVICE

Our transport studies are performed in the modified Malmberg-Penning trap shown in shown in Fig. 1. As in

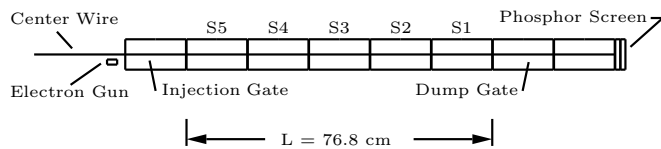


FIG. 1: Schematic of the Occidental College Trap. The usual plasma column is replaced by a biased wire to produce the basic dynamical motions in low density electrons injected from an off-axis gun. The low density and high temperature of the injected electrons largely eliminate collective modifications of the vacuum asymmetry potential. The five cylinders (labeled S1 through S5) are divided azimuthally into eight sectors each.

the standard trap design, a uniform axial magnetic field provides radial confinement of injected electrons, while negatively biased end cylinders (the injection gate and dump gate) provide axial confinement. Our device also operates in the standard inject-hold-dump cycle. A cycle begins by grounding the injection gate which allows electrons from the gun to flow into the central region. This injection gate is then returned to a negative bias which traps the electrons. After a chosen period of time, the dump gate is grounded and the electrons leave the trap and hit a positively biased phosphor screen. Analysis of the images on this screen provides the primary diagnostic.

The principal modification in our device is replacing the usual plasma column with a biased wire running along the axis of the trap. The wire provides a radial electric field to replace the field normally produced by the plasma column and allows the injected low density electrons to have the same zeroth-order dynamical motions (axial bounce and azimuthal $E \times B$ drift motions) as in a standard trap. The lower density (10^5 cm^{-3}) and high temperature (4 eV) of the electrons give a Debye length larger than the trap radius. Under these conditions, potentials in the plasma are essentially the vacuum potentials and previously encountered[6] complications due to collective effects are minimized[2]. Our design also allows the drift rotation frequency $\omega_R(r)$ to be easily adjusted by varying the center wire bias ϕ_{cw} since

$$\omega_R = \frac{-\phi_{cw}}{r^2 B \ln(R/a)} \quad (2)$$

where R and a are the radii of the wall and the center wire, respectively. Despite these changes, the unperturbed confinement time has similar magnitude and shows[7] the same $(L/B)^2$ scaling found in higher density experiments, thus supporting the idea that the radial transport is primarily a single particle process and confirming the relevance of our experiments to standard trap physics.

A unique feature of our device is that the entire confinement region is sectored (five cylinders, labeled S1 through S5 in Fig. 1, with eight azimuthal divisions each). This allows us to apply a simple, known asymmetry by selecting the amplitude and phase of the voltages applied

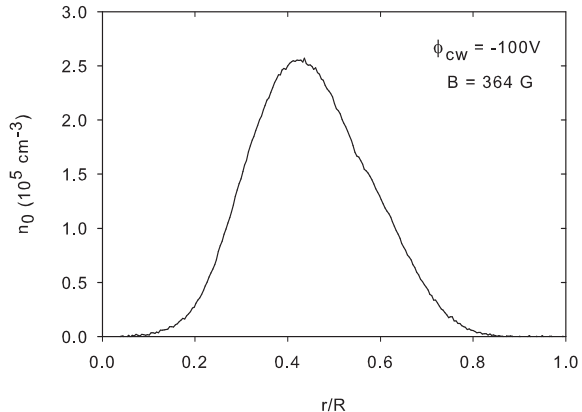


FIG. 2: A typical density profile taken 1600 ms after injection.

to each sector to produce a helical standing wave of the form

$$\phi(r, \theta, z, t) = \phi_W \left(\frac{r}{R}\right)^l \cos\left(\frac{n\pi z}{L}\right) \cos(l\theta - \omega t) \quad (3)$$

where ϕ_W is the asymmetry potential at the wall (typically 0.2 V), R is the wall radius (3.82 cm), L is the length of the confinement region (76.8 cm), n and l are the axial and azimuthal Fourier mode numbers, respectively, and here z is measured from one end of the confinement region. For these experiments $n = l = 1$ and the relative phases of the applied voltages are adjusted so that the asymmetry rotates in the same direction as the zeroth-order azimuthal $E \times B$ drift. For these experiments, the higher order harmonics of the applied asymmetry have amplitudes less than 10% of the fundamental. Since the transport typically scales like the square of the asymmetry amplitude[8], the effect of these harmonics can be ignored.

Data acquisition for these transport studies can be summarized as follows; details have been given elsewhere [2, 8]. Electrons injected into the trap from an off-axis gun are quickly dispersed into an annular distribution. At a chosen time (here, 1600 ms after injection), the asymmetries are switched on for a period of time δt (here, 100 ms) and then switched off. At the end of the experiment cycle, the electrons are dumped axially onto a phosphor screen and the resulting image is digitized using a 512×512 pixel charge-coupled device camera. A radial cut through this image gives the density profile $n_0(r)$ of the electrons. A typical profile is shown in Fig. 2. Shot-to-shot variation in the number of injected electrons is less than 1% and the data is very reproducible. Calibration is provided by a measurement of the total charge being dumped. Profiles are taken both with the asymmetry on and off, and the resulting change in density $\delta n_0(r)$ is obtained. The background transport is typically small compared to the induced transport and

is subtracted off. If the asymmetry amplitude is small enough and the asymmetry pulse length δt short enough, then $\delta n_0(r)$ will increase linearly in time [8]. We may then approximate $dn_0/dt \simeq \delta n_0(r)/\delta t$ and calculate the radial particle flux $\Gamma(r)$ (assuming $\Gamma(r = a) = 0$):

$$\Gamma(r) = -\frac{1}{r} \int_a^r r' dr' \cdot \frac{dn_0}{dt}(r') \quad (4)$$

Here a is the radius of the central wire (0.178 mm). The entire experiment is then repeated for a series of asymmetry frequencies ω and the resulting flux versus radius and frequency data saved for analysis.

III. EXPERIMENTAL RESULTS

It is easy to show experimentally that the transport depends separately on both ω and ω_R and that the form of the transport equation is more complicated than a simple Fick's Law dependence $\Gamma = -D\nabla n_0$. Typical data are shown in Figs. 3 and 4. In Fig. 3a we plot the radial particle flux Γ versus radius r for three representative asymmetry frequencies ω to illustrate the dependence on ω . In Fig. 3b the same data is plotted versus density gradient ∇n_0 to show that there is no simple relationship between Γ and ∇n_0 . Similarly, Fig. 4 shows the same plots for three values of the center wire bias ϕ_{cw} (and thus of ω_R). Again, no simple analysis of this data is evident.

We now apply the hypothesis that ω and ω_R always enter the transport physics in the combination $\omega - l\omega_R$. We take Γ vs r data for a number (typically 26) of asymmetry frequencies ω . Since $l = 1$ in our experiments, these frequencies are chosen to be within the range of ω_R values, i.e., $\omega_R(R) < \omega < \omega_R(a)$. We then select from this Γ vs r vs ω dataset those points where $\omega - l\omega_R = 0$, thus insuring that any function of this combination is constant. We do this as follows: for each experimental value of ω , we determine the radial position r_{sel} where $\omega - l\omega_R = 0$, interpolating between data points if necessary. We then take from the Γ vs r data for that ω the single flux value Γ_{sel} that occurs at r_{sel} . After this is repeated for each ω , we have Γ_{sel} vs r_{sel} with r_{sel} spanning the range of radius values. Since the plasma parameters are independent of ω , ∇n_0 does not change with ω and we can also form Γ_{sel} vs ∇n_0 .

When the selected flux is plotted versus the density gradient ∇n_0 , a roughly linear dependence is observed and this dependence is roughly independent of the center wire bias ϕ_{cw} . This data is shown in Fig. 5 for four values of the axial magnetic field B . The linearity of the individual plots shows that the selected flux has the form $\Gamma_{sel} = m\nabla n_0 + \Gamma_0$, where m and Γ_0 are constants for a given B . In particular, m and Γ_0 are not functions of ω or ω_R . The first follows from the fact that the data points in Fig. 5 are all at different frequencies and the second follows from the lack of dependence on ϕ_{cw} . Since we

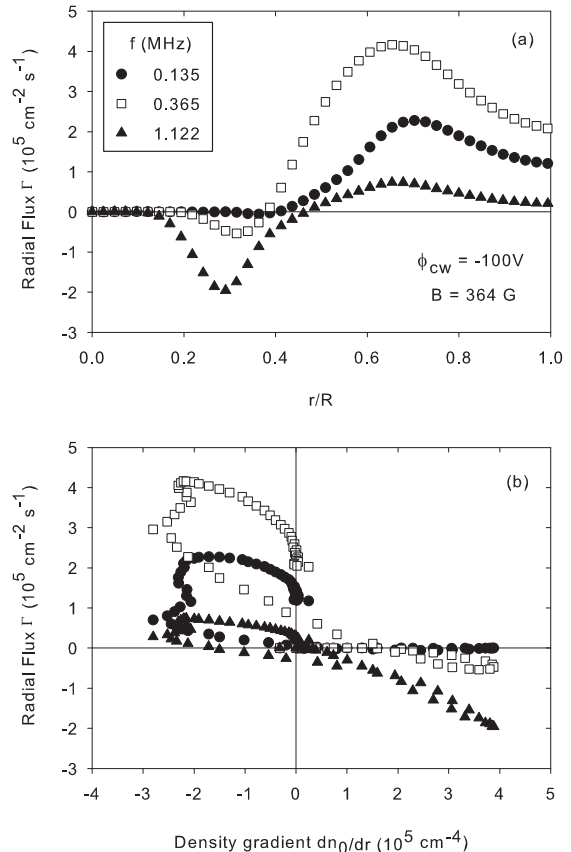


FIG. 3: (a) Plot of typical flux versus scaled radius data for three representative asymmetry frequencies. (b) Plot of the same flux data versus density gradient. The number of plotted points has been adjusted for clarity. The plots show that the flux depends on the asymmetry frequency and does not follow a simple Fick's Law dependence on density gradient.

know from Figs. 3 and 4 that, in general, the flux depends separately on both ω and ω_R , the independence of Γ_{sel} on these quantities supports our hypothesis that they enter the physics only in the combination $\omega - l\omega_R$. We also note that, since the points in Fig. 5 come from different radii, m and Γ_0 are not strong functions of r either, although the deviations from linearity may indicate a weak dependence on r .

Finally, the slope of a least-squares fitted line to the plots in Fig. 5 then gives the quantity m . For the four values of magnetic field, we find $m \propto B^{-1.33 \pm 0.05}$ as shown in Fig. 6. A similar procedure using the y-intercept of the fitted lines gives $\Gamma_0 \propto B^{-1.13 \pm 0.10}$.

IV. DISCUSSION

The magnetic field scalings for m and Γ_0 are similar enough to consider a common scaling for both. This is

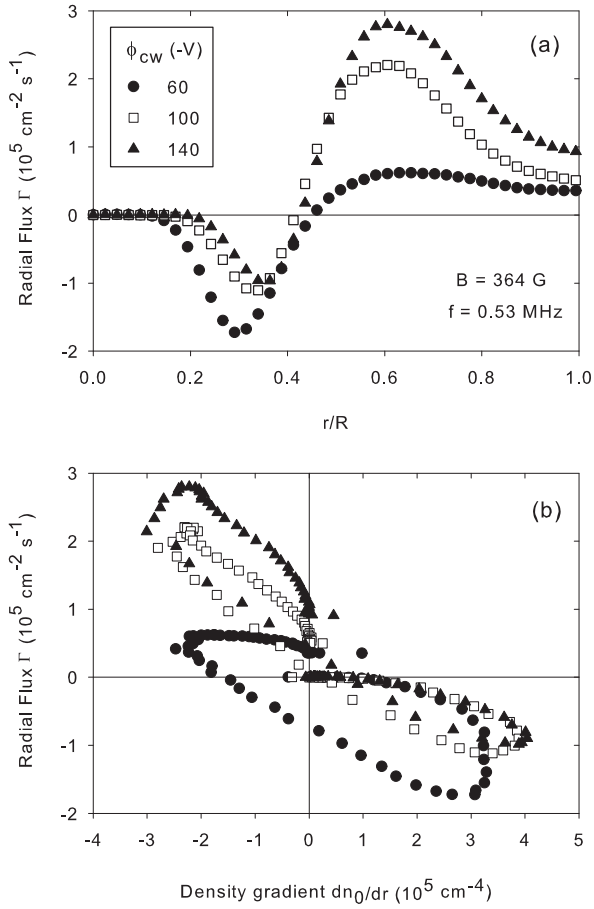


FIG. 4: (a) Plot of typical flux versus scaled radius data for three representative values of the center wire bias ϕ_{cw} . (b) Plot of the same flux data versus density gradient. The number of plotted points has been adjusted for clarity. The plots show that the flux depends on the rotation frequency (since $\omega_R \propto \phi_{cw}$ and, again, does not follow a simple Fick's Law dependence on density gradient.

of interest for comparison with the common theoretical form for the flux. In Fig. 7 we apply a scaling of $B^{1.33}$ to all the data of Fig. 5 and obtain a universal curve of the form $(B/B_0)^{1.33}\Gamma_{sel} = -D_0(\nabla n_0 + f_0)$, where $B_0 = 233 \text{ G}$ is a conveniently selected constant. A least-squares fit to the scaled data gives $D_0 = 1.00 \text{ cm}^2 \text{ s}^{-1}$ and $f_0 = 1.01 \times 10^5 \text{ cm}^{-4}$. Note that this magnetic field scaling does not match the B^{-2} plateau regime scaling predicted by Eq. (1), the more complicated B -scaling of the banana regime[3], or any other theoretical scaling of which we are aware. The low electron-electron collision frequency of our experiment would put us in the banana regime.

Of course, our universal curve only gives the flux for points where $\omega - l\omega_R = 0$. It does, however, allow us to say something about the form of the general flux equation. Our data tell us that the general flux must be a

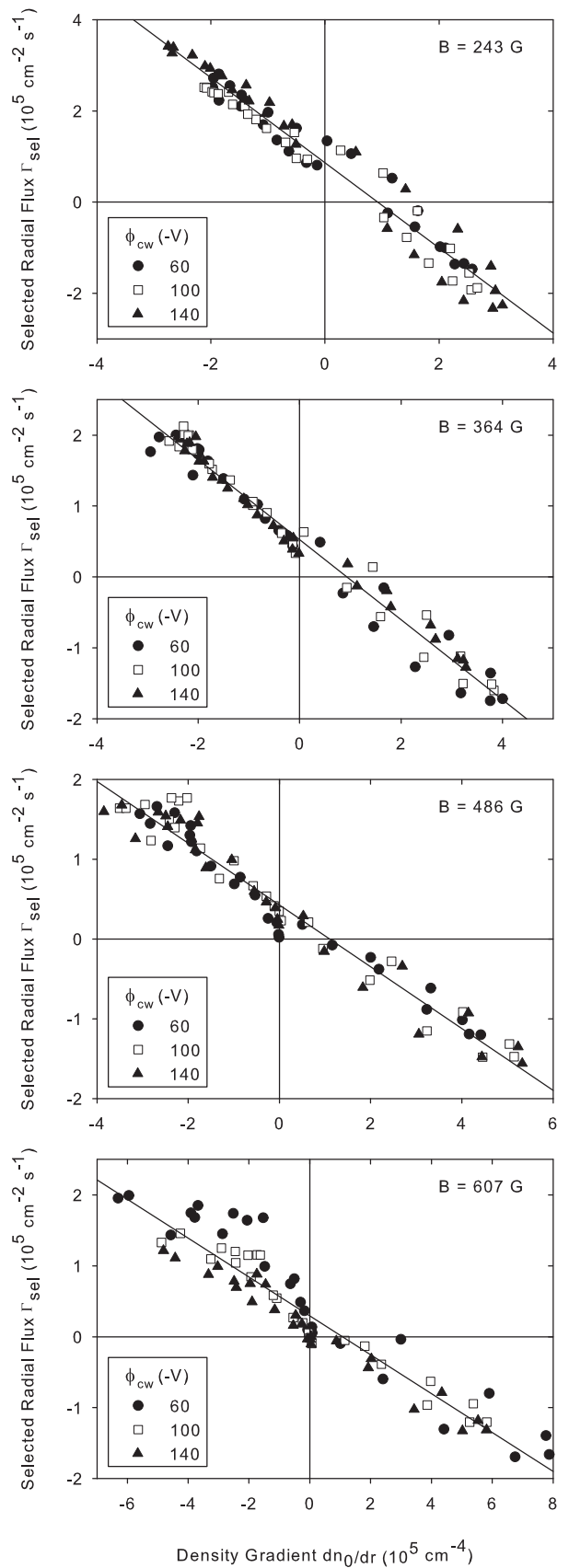


FIG. 5: Selected flux versus density gradient with center wire bias as a parameter. The four graphs show data for four values of the magnetic field. The slope of a fitted line gives the diffusion coefficient.

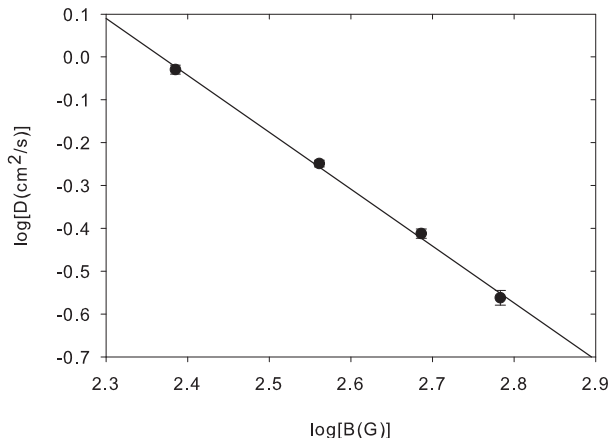


FIG. 6: Log-log plot of the diffusion coefficient (determined from the plots in Fig. 5) versus the axial magnetic field B . A least squares fit to the data gives $D \propto B^{-1.33 \pm 0.12}$.

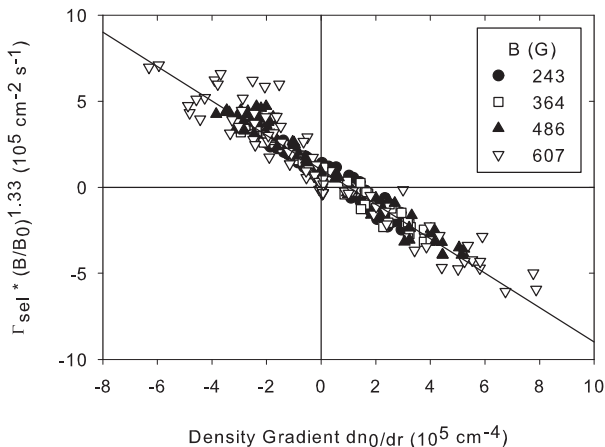


FIG. 7: A universal curve results when the selected flux data of Fig. 5 is multiplied by a scaling factor $(B/B_0)^{1.33}$ and plotted versus the density gradient dn_0/dr .

function of $\omega - l\omega_R$ and that the flux equation must reduce to the equation for Γ_{sel} when $\omega - l\omega_R = 0$. Without further information, we must thus allow both D_0 and f_0 to become functions of $\omega - l\omega_R$:

$$\Gamma = -(B_0/B)^{1.33} D(\omega - l\omega_R) [\nabla n_0 + f(\omega - l\omega_R)] \quad (5)$$

where $D(\omega - l\omega_R = 0) \equiv D_0$ and $f(\omega - l\omega_R = 0) \equiv f_0$. Note that, except for the magnetic field scaling, the form of this equation is consistent with Eq. (1).

Although the plots of Γ_{sel} vs ∇n_0 in Fig. 5 all show a

linear trend, there remains some deviation from linearity in the data, part of which appears systematic. We have considered two possible sources for this deviation. The first involves the adjustment the value of ω_R due to end effects. In selecting the data points where $\omega - l\omega_R = 0$, we have used the infinite length expression for ω_R given by Eq. (2). In fact, the radial electric field (and thus, ω_R) is a function not only of r but also z due to variations at the ends of the confinement region, and the penetration of a particle into these end regions depends on the particle energy. We have estimated the size of this correction (see appendix) and it is not large enough to explain the scatter in the data.

A second possible source of the data scatter is heating of the plasma during the application of the asymmetry. This is predicted theoretically[9] and observed in other experiments[10]. While the low density of our plasma makes it difficult to obtain accurate temperature data using the standard technique[11], our measurements do indicate that some heating occurs, particularly at the higher asymmetry frequencies. This may account for the deviation from linearity.

V. CONCLUSION

We have applied a new experimental technique to study the magnetic field dependence of asymmetry-induced transport in a modified Malmberg-Penning trap. The technique allows us to remove the ω_R -dependence from our data and thus isolate the remaining magnetic field dependence. The technique works reasonably well and gives a diffusion coefficient that scales like $B^{1.33}$. This scaling does not match that of any known theory.

Acknowledgments

This material is based upon work supported by the Department of Energy under award number DE-FG02-06ER54882.

APPENDIX A: ESTIMATE OF ROTATION FREQUENCY CORRECTIONS TO DUE TO END EFFECTS

The confining end potentials of our trap will alter the radial electric field seen by the electrons as they traverse the trap and thus produce a rotation frequency that is different from the infinite length expression given in Eq. (2). To estimate this correction, we consider the rotation caused by the end potentials alone (i.e., with the center wire bias set to zero). The actual end potential $\phi_{end}(r, z)$ is an infinite sum involving decaying exponentials in z and Bessel functions in r with arguments adjusted to match the boundary conditions

$\phi_{end}(a, z) = \phi_{end}(R, z) = 0$. Because the confining potential (typically -140 volts) is large compared to the electron energy, the electrons will be reflected at relatively large values of z where $\phi_{end} \approx kT/e$. The infinite sum can then be approximated by the first term, which has a single maximum in radius. For the purpose of this estimate, we replace the cumbersome Bessel function expression by a sine function with the same general behavior

$$\phi_{end} \approx \frac{kT}{e} \sin\left(\pi \frac{r-a}{R-a}\right). \quad (\text{A1})$$

Since the end potential falls off in z with a scale length R , we take the interaction time with the end potential to be R/\bar{v} . Calculating the azimuthal $E \times B$ drift then gives

$$\theta_{end} \approx \frac{\pi R k T}{r e B \bar{v} (R-a)} \cos\left(\pi \frac{r-a}{R-a}\right). \quad (\text{A2})$$

If we conservatively let the cosine take its maximum value and note that $R-a \approx R$ we obtain

$$\theta_{end} \approx \frac{\pi k T}{r e B \bar{v}}. \quad (\text{A3})$$

We now compare this end drift with that produced by the center wire potential during one axial bounce, θ_{cw} . The interaction time is now L/\bar{v} and ω_R is given by Eq. (2). We obtain

$$\frac{\theta_{end}}{\theta_{cw}} \approx \frac{\pi k T}{e \phi_{cw}} \frac{r}{L} \ln(R/a). \quad (\text{A4})$$

Letting r have its maximum value R and taking typical values $kT = 4$ eV and $e\phi_{cw} = 100$ eV, we get $\theta_{end}/\theta_{cw} \approx 3\%$. Thus, the additional azimuthal drift produced by the end potentials is small for our experiment.

-
- [1] For a sampling of current work, see the papers in *Non-Neutral Plasma Physics VI*, edited by Michael Drewsen, Ulrik Uggerhøj, and Helge Knudsen, American Institute of Physics, Melville, N.Y. (2006).
- [2] D.L. Eggleston and B. Carrillo, Phys. Plasmas **10**, 1308 (2003).
- [3] D. L. Eggleston and T. M. O'Neil, Phys. Plasmas **6**, 2699 (1999).
- [4] J. Notte and J. Fajans, Phys. Plasmas **1**, 1123 (1994).
- [5] J. M. Kriesel and C. F. Driscoll, Phys. Rev. Lett. **85**, 2510 (2000).
- [6] D. L. Eggleston, T. M. O'Neil, and J. H. Malmberg, Phys. Rev. Lett. **53**, 982 (1984).
- [7] D.L. Eggleston, Phys. Plasmas **4**, 1196 (1997).
- [8] D. L. Eggleston and B. Carrillo, Phys. Plasmas **9**, 786 (2002).
- [9] Roy W. Gould, in *Non-Neutral Plasmas III*, edited by John J. Bollinger, Ross L. Spencer, and Ronald C. Davidson, (American Institute of Physics, Melville, N.Y., 1999), p. 170.
- [10] J. R. Danielson, C. M. Surko, and T. M. O'Neil, Phys. Rev. Lett. **99**, 135005 (2007).
- [11] D.L. Eggleston, C.F. Driscoll, B.R. Beck, A.W. Hyatt, and J.H. Malmberg, Phys. Fluids B, **4**, 3432 (1992).